http://pubs.acs.org/journal/aelccp

Photoelectrode Fabrication and Modular PEC Reactor Integration for Stable Solar Hydrogen Production

Ingrid Rodríguez-Gutiérrez,* Lizandra R. P. Peregrino, Gabriel H. Morais, Francine Coa, Diego Stéfani Teodoro Martinez, Renato V. Gonçalves, and Flavio L. Souza*



Downloaded via UNIV OF SAO PAULO on October 10, 2025 at 12:28:09 (UTC). See https://pubs.acs.org/sharingguidelines for options on how to legitimately share published articles.

Cite This: ACS Energy Lett. 2025, 10, 4769-4776



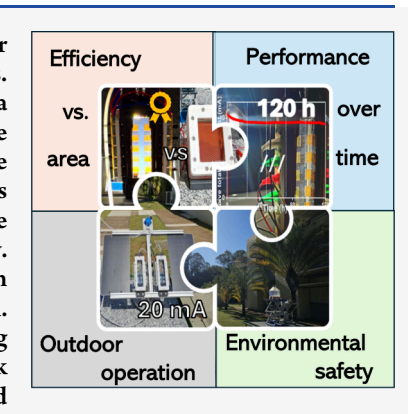
ACCESS I

Metrics & More

Article Recommendations

Supporting Information

ABSTRACT: Photoelectrochemical (PEC) water splitting is a promising route for solar hydrogen production, yet scalability and environmental safety remain key challenges. Here, we present a modular PEC platform using hematite photoelectrodes fabricated via a scalable polymeric precursor method with uniform Al/Zr comodification to enhance charge transport and adhesion. A total of 100 reproducible photoelectrodes were produced and characterized using customized PEC cells with two different active areas (0.28 and 1 cm²) to assess scale-dependent performance. Ten photoelectrodes were integrated into each 3D-printed reactor, demonstrating an effective small-scale assembly. Ten such reactors could form a 100 cm² module, supporting scalable deployment. Each reactor delivered stable photocurrents (~10 mA at 1.23 $V_{\rm RHE}$) for over 120 h under 1 sun. Outdoor operation of two series-connected reactors reached 20 mA. Ion leaching remained below national discharge limits, confirming environmental safety. This work establishes a scalable, stable, and modular PEC strategy, advancing hematite-based devices toward real-world solar hydrogen production.



Photoelectrochemical (PEC) water splitting enables direct solar-driven hydrogen production, with the potential for bias free or low bias operation through integrated photoelectrodes or tandem configurations. ^{1–6} PEC device architectures range from single photoelectrodes paired with dark counter electrodes (Figure S1a,b) to tandem designs that incorporate either complementary photoelectrodes (Figure S1c) or a photovoltaic device to assist water splitting (Figure S1d). ^{7–10} While numerous studies have demonstrated promising solar-to-hydrogen efficiencies using advanced photoabsorbers, the translation to large area, into durable, scalable devices remains a major barrier to practical implementation. Most PEC technologies remain at low technology readiness levels (TRL < 4) due to limitations in device scalability, long-term operational durability, and environmental safety. ⁸

Material optimization efforts have mostly focused on semiconductors such as metal oxides and III—V compounds, employing strategies such as nanostructuring, doping, surface passivation, and heterojunction design. However, many of these advances rely on fabrication techniques that are not easily transferable to large area systems or are incompatible with cost-effective processing. In addition, integration-related losses, including increased ohmic resistance, poor thermal dissipation, and gas management issues, are not often addressed systematically. ^{14–18} In recent years, the development

of reactor architecture has emerged as a critical factor in bridging the gap between materials innovation and practical implementation (Figure S2). The first prototype-scale PEC water splitting device was reported in 2011 marking the start of gradual progress in PEC technologies. 19 According to the Web of Science, only 59 articles on scaled PEC systems were published by December 2024 (Figure S2a,b). Between 2011 and 2019, publication rates remained low (2.2 articles/year), but interest has grown steadily since 2020, reaching an average of 7.8 articles/year (Figure S2b). Table S1 summarizes key experimental reports illustrating efforts aimed at transitioning from laboratory scale efficiency to real world implementation. Photoabsorbers such as WO₃ (tungsten trioxide), $^{19-21}$ α -Fe₂O₃ (hematite), 15,17,18,22 and BiVO₄ (bismuth vana- $(a)^{23-27}$ have been tested across device areas from 15 to 16,000 cm² under varying illumination, pH, and applied bias (1-12.8 suns, pH 0.3-13.6, 0.6-1.73 V_{RHE}). Among leading

Received: July 25, 2025 Revised: August 25, 2025 Accepted: August 29, 2025 Published: September 6, 2025





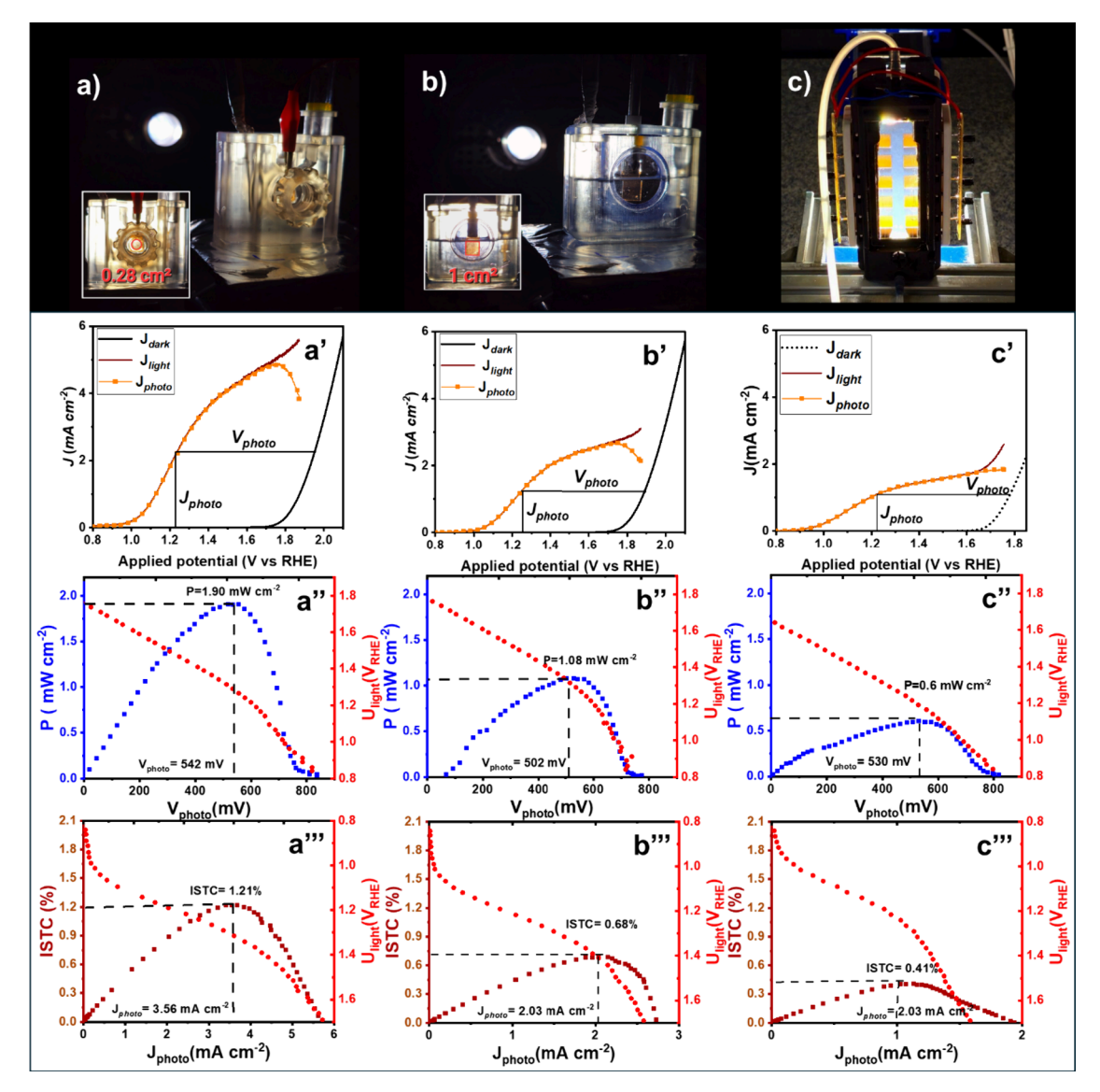


Figure 1. a, b, c) Photoelectrochemical cells and reactor employed in this work for the assessment of PEC water splitting activity curves at different total photoabsorber area scales of 0.28 cm², 1 cm², and 10 cm², respectively. a', b', c') i–V curves obtained in the dark (black line) and under simulated solar illumination (AM 1.5 G, 100 mW cm⁻², red line) and the generated photocurrent, J_{photo} (orange line) at mentioned areas. a", b", c") Intrinsic photovoltaic power as a function of the photopotential for the correspondent area. a", b", c") Intrinsic solar-to-chemical conversion efficiency (ISTC) efficiency as a function of the photocurrent density measured for each correspondent area. The secondary y axis on the right represents the applied potential (U_{light}) with respect to the reference electrode.

contributions, Mendes and co-workers have advanced integrated PEC systems by optimizing reactor architecture, solar concentration, and thermal and gas management. Their work demonstrates that modular configurations composed of multiple small area photoelectrodes can effectively mitigate ohmic losses and support long-term operation, one of the most critical bottlenecks in PEC scale-up. ²⁹

Scaling PEC technologies requires fabrication strategies that are both cost-effective and reproducible across large surface areas. Hf⁴⁺ modification in hematite demonstrates the importance of targeted dopant incorporation in optimizing the photoelectrode performance. At the grain boundaries, the controlled distribution of Hf⁴⁺ reduces interfacial resistance by lowering energy barriers, thereby facilitating electron hopping across grains, a key transport mechanism in hematite. In parallel, Hf⁴⁺ enhances adhesion at the photocatalyst/TCO

interface, promoting more efficient electron collection and injection into the external circuit. As a result, large-area photoanodes (15.75 cm²) exhibited only a 12.3% performance loss compared to their lab-scale counterparts, underscoring the critical role of dopant positioning in scaling device efficiency.¹⁷ Our group employs a polymeric precursor solution approach that enables compositionally controlled doping and morphology tuning in hematite photoelectrodes. 30-33 At laboratory scale (0.28 cm²), Al³⁺ and Zr⁴⁺ modified hematite electrodes have achieved photocurrent densities >6.0 mA cm⁻² at 300 mV overpotential under 1 sun (AM 1.5G) illumination.³⁴ To address the persistent challenge of scaling PEC devices without compromising performance, the present study evaluates a modular PEC architecture built from 100 reproducible Al/Zrdoped hematite photoelectrodes deposited onto 2 × 1 cm² sized F-doped tin oxide glass substrates (Figure S3). Intrinsic photoelectrochemical behavior was evaluated across varying

ACS Energy Letters http://pubs.acs.org/journal/aelccp Letter

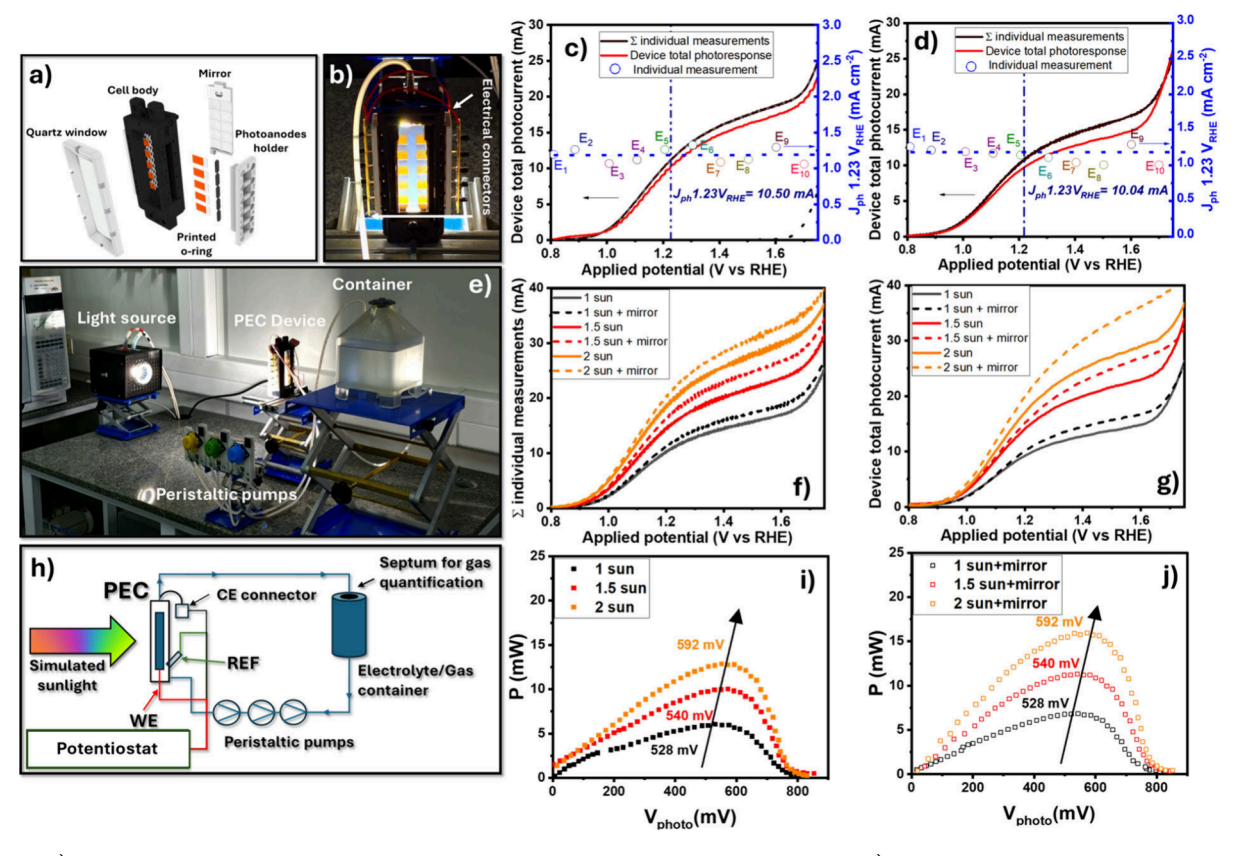


Figure 2. a) Exploded view of the modular reactor using hematite as the photoelectrode. b) Photograph of the real reactor with all components. c,d) Comparison between the measured device total photocurrent (solid red line) and the summation of the individual measurements (1 cm², solid black line) of two different ensembled reactors (named as reactors 1 and 2, respectively). Right axis represents the photocurrent density obtained in the individual measurements at the thermodynamic water oxidation potential. e) Experimental setup of the PEC cell coupled to solar simulator with the respective process flow diagram (h) displaying electrolyte recirculation. f) Summation of individual measurements at different light intensities. g) i-V curves displaying the device total photocurrent as a function of applied potentials at different illumination conditions. Intrinsic photovoltaic power as a function of the photopotential for different illumination conditions in the absence (i) and the presence (j) of a mirror as optical reflector.

active areas under controlled conditions to examine performance, quantify scaling losses, and guide reactor integration. This information enabled the development of a modular reactor for long-term stability, outdoor field testing, and environmental safety assessment—key parameters for deployment-oriented PEC design.

To evaluate scale-dependent performance, photoelectrochemical responses at different active areas (0.28 cm² and 1 cm²) were compared under standardized conditions using customized PEC cells that precisely exposed only the specified areas to light and electrolyte (Figure 1a-c). Al/Zr-modified hematite photoelectrodes (~100 nm thick) were synthesized via a polymeric precursor route that guarantees uniform composition, reproducible dopant incorporation, and strong adhesion across all samples with a total of 100 electrodes prepared. These photoelectrodes serve as the basis for areadependent performance and reproducibility evaluation. Photoelectrochemical performance was evaluated under simulated AM 1.5G illumination (100 mW cm $^{-2}$, 25 °C) and in the dark. In the dark, no current was observed until 1.80 V_{RHE}. Under illumination at 0.28 cm² (Figure 1a), Al/Zr-modified photoelectrodes showed a photocurrent onset of 0.97 \pm 0.04 V_{RHE} and $J_{@1.23VRHE}$ of 2.26 ± 0.35 mA cm⁻². Scaling to 1 cm² (Figure 1b) maintained the onset potential at 1.01 ± 0.02 V_{RHE} , but $J_{@1.23VRHE}$ declined to 1.28 \pm 0.17 mA cm⁻², a 43% loss with this 4-fold area increase, mainly from ohmic losses. As

commonly observed during scaling-up, a decrease in performance is often recorded for larger active areas, and it is primarily associated with ohmic loss. 15 Although mitigation of scalingrelated losses is beyond the scope of this work, previously reported strategies are being evaluated for integration into future device iterations. 17,27 An 800 mV shift between the photocurrent onset and electrochemical onset was observed. To further analyze performance, we used the Dotan et al. method to extract intrinsic solar-to-chemical conversion from i-V curves under light and dark (Figure 1). 35,36 For 0.28 cm², the maximum power output was 1.90 mW cm $^{-2}$ at 1.40 V_{RHE} $(V_{photo} = 542 \text{ mV}; \text{ Figure 1a}^2); \text{ for 1 cm}^2, \text{ the maximum power}$ was 1.08 mW cm⁻² at 1.39 V_{RHE} (V_{photo} = 502 mV; Figure 1b"). Intrinsic solar-to-chemical conversion efficiency (ISTC) decreased from 1% (3.56 mA cm⁻²) to 0.7% (2.03 mA cm⁻²) as the area increased. These currents were achieved only at 2.01 and 1.93 V_{RHE} in the dark, reflecting a \sim 600 mV overpotential decrease. Notably, the fill factor improved from 52% to 59% upon scaling.

Given the performance decay in hematite photoelectrodes upon scaling is mostly associated with the increased ohmic resistance and limited charge transport, ^{15,37} modular device design presents a viable strategy to mitigate these limitations by minimizing lateral resistance. ²² A custom PEC reactor (Figure 1c and Figure 2) was developed to host ten photoelectrodes, each with a geometric area of 1 cm², enabling

ACS Energy Letters http://pubs.acs.org/journal/aelccp Letter

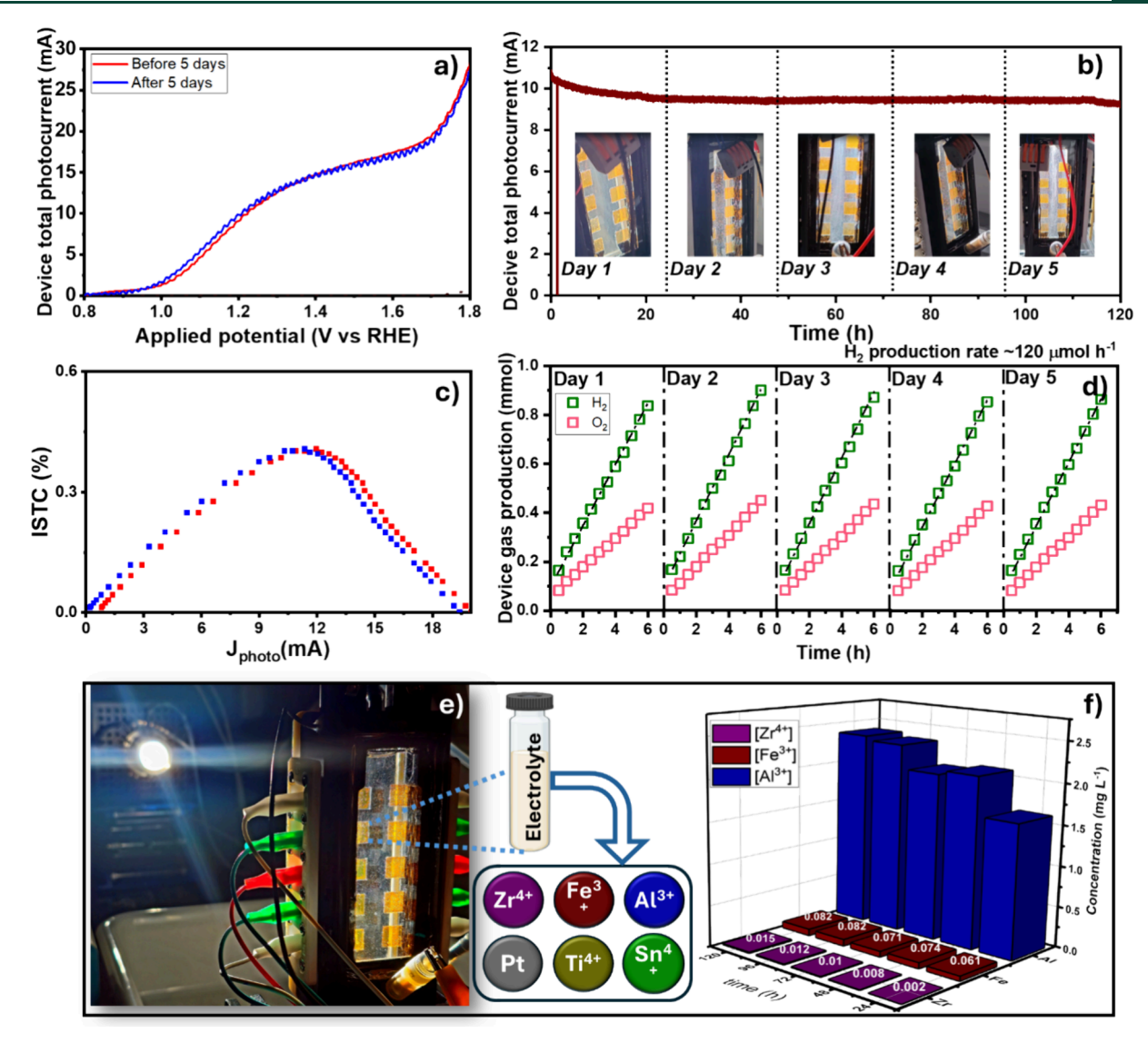


Figure 3. a) Device total photocurrent as a function of applied potential before and after stability measurements. b) Long-time stability measurement performed at 1.23 V_{RHE} over 120 h. The photographs were taken each 24 h during the experiment. c) *ISTC* as a function of total photocurrent before and after stability measurements. d) Gas evolution quantification recorded 6 h per day for 5 consecutive days. The Reactor was operated under 1 sun illumination and an electrolyte flow rate of 1 mL s⁻¹ using NaOH 1 M as electrolyte solution. e) PEC reactor operation and elements monitored for 5 days. f) Element concentration as a function of time determined by ICP-OES.

reliable evaluation under controlled conditions. This architecture was designed to preserve current density across larger areas and enable performance benchmarking under standardized conditions (see Supporting Information section 1 for details). The reactor body was fabricated via 3D printing using high chemical and thermal resistance resin to ensure durability during operation (Figure 2a). A quartz window, secured with screws, served as the illumination interface, while the back window was directly bonded to the reactor frame to ensure stability and alignment. Custom O-rings (Flexible 80A resin) conformed to photoelectrode geometry, maintaining uniform seals. The design includes a single inlet/outlet to facilitate continuous electrolyte flow and gas removal. Photoelectrodes were accommodated to ensure uniform illumination (Figure 2b) and could optionally incorporate a rear mirror to enhance the photon absorption. A Ti mesh counter electrode coated with Pt (NovaCell) was used for charge collection. Gold clips provided low-resistance electrical connections between electrodes, enabling reliable series integration. A photograph of the

complete PEC setup and corresponding flow schematic is shown in Figures 2e and 2h, respectively. A step-by-step assembly guide and full component list are provided in Figure S4 and Supporting Information section 1. Under 1 sun illumination (for calibration settings see Figure S5), the reactor achieved a $J_{@1.23\text{VRHE}}$ of 10.05 mA (1.05 mA cm⁻², Figure 1c'). Consistent with the methodology applied to smaller areas, J_{vhoto} , V_{vhoto} , P, and ISTC were calculated (Figure 1c"and 1c"). The PEC reactor achieves a maximum power output of 6 mW (0.6 mW cm⁻²) and an ISTC of 0.41% corresponding to 56% and 60% of the values obtained for 1 cm² active area, respectively. These values were obtained at an applied potential close to the water oxidation potential ($U_{light} = 1.26$ V_{RHE}). A fill factor of 51% is obtained for a 10 cm² active area, indicating a moderate increase in ohmic losses compared to smaller area cells. Reported values for scaled hematite photoelectrodes typically range around 0.45 to 0.65 mA cm⁻² under 1 sun and bias equal to or higher than 1.45 V_{RHE} , with a maximum near 2 mA cm⁻² achieved only

ACS Energy Letters http://pubs.acs.org/journal/aelccp

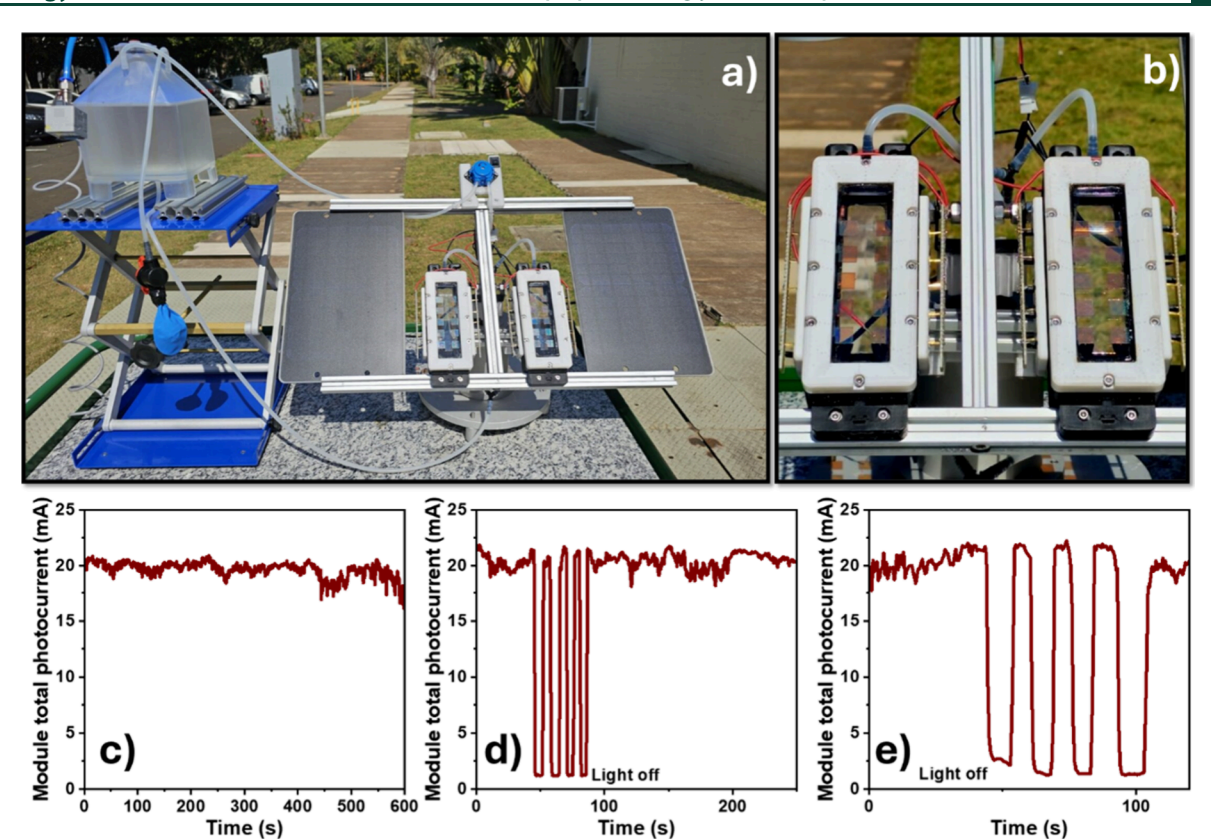


Figure 4. Outdoor measurements of modular PEC reactors. a) Photograph of the device with all components. (b) Close-up photograph of two assembled reactors. (c-e) Chronoamperometry curves of modular PEC reactors under outdoor illumination.

under concentrated illumination conditions (up to 12.8 suns). ¹⁸ Considering the total device area (135 cm²), including housing, the power density decreases to 0.04 mW cm², highlighting the impact of the device footprint on practical performance. Such limitations, frequently attributed to nonuniform charge extraction, restricted light absorption across large areas, and interface instability, represent a challenge toward real-world PEC implementation.

Operational consistency and reproducibility were evaluated by assembling and independently testing two modular PEC reactors under standardized laboratory conditions. The photocurrent density of each reactor under 1 sun was benchmarked against the average i-V response of their constituent photoelectrodes (Figure 2c,d). Reactor 1 achieved 10.5 mA at 1.23 V_{RHE} (92% of the projected maximum, calculated from the sum of individual measurements; see Figure S6), while Reactor 2 reached 10.04 mA (\sim 88%), indicating high efficiency and reproducibility across setups. Operational enhancements were explored by using two strategies: rear reflection and increased illumination intensity. A quartz back window enabled insertion of a reflective mirror behind the photoelectrodes as an optical reflector to improve photon recycling and minimize optical losses. Illumination intensity was incrementally increased to 1.5 and 2 suns using a calibrated solar simulator. Projected and measured photocurrent values both increased with illumination intensity (Figure 2f,g). The reactor's intrinsic photovoltaic power peaked at 12.84 mW under 2 suns and rose to 15.93 mW with a rear mirror (Figure 2i,j); in both scenarios, V_{photo} increased with illumination, indicating enhanced voltage compensation under higher light flux. Maximum ISTC (Figure S7) was observed at 1.5 suns (0.4%), in agreement with

calculated solar-to-hydrogen (STH) efficiency (Figure S8), suggesting charge carrier utilization becomes limited at higher intensities, likely due to increased bimolecular recombination at higher charge carrier densities. 39,40 Thermal effects at elevated illumination may also influence electrolyte properties or introduce resistive losses; however, 24 h experiments at varied electrolyte flow rates (Figure S9) showed no significant effect, confirming reactor stability and effective mitigation of flow related issues. Incorporating a rear mirror (Figure S10a) yielded a slight but measurable increase in the photocurrent (Figure S10b) and a shift in the ISTC trend, now rising with light intensity. This enhancement results from the mirror redirecting unabsorbed photons back to the photoelectrodes, increasing the photon flux and light utilization (Figure S11). By recovering reflected light, this strategy compensates for optical losses in thin films, explaining the improvement in photoresponse.

The reactor long-term operational stability was evaluated under continuous 1 sun illumination at 1.23 V_{RHE} over 120 h under a constant electrolyte flow (1 mL s⁻¹) (Figure 3 and video Supporting Information). One sun was selected as the standard illumination to ensure consistent, real world relevant conditions. Lamp intensity drift (Figure S12a) was monitored and used to normalize photocurrent data (Figure S12b). Photocurrent decay remained below 5% throughout the test, indicating a stable performance (Figure 3b). *LSV* and *ISTC* curves before and after the experiment confirmed minimal degradation (Figure 3a,c). XPS analysis before and after the 120 h test showed no significant changes in Fe, Al, or Zr surface composition on the hematite photoelectrodes (Figure S13), while only minor variation in the O 2p spectra was observed, likely due to surface hydration. Moreover, gas

Letter

chromatography measurements over 6 h per day across 5 days revealed a stable hydrogen evolution rate of $\sim 120~\mu \text{mol h}^{-1}$ under 1 sun and 1 mL s⁻¹ flow. A Faradaic efficiency near 83% indicates the need for further optimization of the reactor design to enhance gas extraction and improve hydrogen evolution rates. Even so, these results indicate that the system sustains photoelectrochemical activity, supporting its potential for real world deployment and reliability benchmarking.

While photocurrent and XPS analyses before and after 120 h of operation confirmed the photoelectrode's structural integrity, further evaluation was conducted to quantify potential electrode leaching, especially under conditions simulating prolonged use or improper disposal (Figure 3e,f). Electrolyte samples collected throughout the 120 h test were analyzed via ICP-OES to detect leaching of Al3+, Zr4+, Fe3+, Pt, Ti⁴⁺, and Sn⁴⁺ ions, with Al³⁺, Zr⁴⁺, Fe³⁺, and Sn⁴⁺ potentially originating from the photoelectrode (photoabsorber layer and FTO/aluminum borosilicate glass substrate), while Pt and Ti⁴⁺ ions arise from the counter electrode (Figure 3e). ICP-OES results (Figures 3f, S14a) showed negligible release of Zr⁴⁺, Fe³⁺, Pt, and Ti⁴⁺ (<0.1 mg L⁻¹), with values comparable to blank FTO control electrodes (Figure S14b,c). However, Al³⁺ and Sn^{4+} concentrations reached 2.38 mg L^{-1} and 3.13 mg L^{-1} , respectively, after 120 h, stabilizing after 96 h. Considering the electrolyte volume and the deposition method, the maximum amount of Al3+ introduced as a dopant into the hematite structure during fabrication—that could be released from the photoelectrodes—is approximately 0.3 mg L⁻¹. This value matches the Al³⁺ level measured over 120 h using the substrate alone in place of the photoelectrodes (Figure S14). This suggests that a significant portion of the Al3+ signal may originate from the aluminum borosilicate glass substrate itself, as previously reported. Therefore, the Al3+ detected in the electrolyte is more plausibly attributed to leaching from the substrate rather than from the hematite photoelectrode. In this line, Sn⁴⁺ levels were significantly lower than in the FTO blank (124.4 mg L^{-1}), likely due to the protective hematite layer. Considering potential environmental impacts, we compared observed metal ion concentrations to Brazilian regulatory standards (CONAMA Resolution 430/2011). The maximum Fe³⁺ concentration detected (0.082 mg L⁻¹) is well-below the permissible limit for effluent discharge (15 mg L⁻¹). Although the regulation does not specify discharge limits for zirconium or aluminum, both can be efficiently removed via pH adjustment and precipitation prior to disposal, mitigating ecological risks.

Scalability and real world applicability of the PEC reactor were monitored by integrating two reactors in series and testing them under outdoor conditions in Campinas, Brazil (Figure 4a,b), where average solar irradiation reaches ~ 5153 Wh m⁻² per day.⁴¹ Operated at 1.23 V_{RHE}, the system delivered a stable photocurrent of 20 mA throughout the test period (Figure 4c-e), with minor fluctuations corresponding to natural variations in solar irradiation. Light chopper measurements confirmed that the recorded current originated from reactor operation, demonstrating the system's responsiveness under dynamic light conditions. Overall, the modular architecture, based on independently fabricated hematite photoelectrodes, enabled scalable integration, while highlighting the performance trade-offs associated with increased active areas. Indoor characterization established key benchmarks for photocurrent density, fill factor, and stability over 120 h, while optical enhancement via rear reflection further

improved the device efficiency. ICP-OES analysis confirmed low ion leaching throughout the extended operation, and environmental thresholds remained well-below national discharge limits, supporting safe implementation. Outdoor operation under real conditions corroborated the reactor's promise: although a decrease in photocurrent compared to the sum of individual photoelectrodes is evident (probably associated with resistive losses and interconnection limitations), the assembly demonstrates that charge collection engineering is necessary for overcoming the bottlenecks in scale-up. Scalable device architecture, reproducible photoelectrode synthesis, and modular integration must be addressed to advance PEC systems toward deployment. Future development will require multilevel optimization (photoabsorber selection, catalyst pairing, electrode interconnection, electrolyte management, and thermal control) to meet application-specific targets. The integrated methodology demonstrated here provides a foundation for translating labscale PEC innovation into practical, real-world hydrogen production systems.

ASSOCIATED CONTENT

Supporting Information

The Supporting Information is available free of charge at https://pubs.acs.org/doi/10.1021/acsenergylett.5c02340.

Detailed experimental procedures for photoelectrode fabrication, modular PEC reactor assembly, photoelectrochemical characterization under indoor and outdoor conditions, and long-term stability testing. Additional figures provide schematics of PEC device architecture, a literature survey on scale-up efforts, photographs of synthesized electrodes and device components and calibration tools. Performance related data includes i-V curves for individual electrodes, ISTC efficiency under variable illumination and mirror use, calculated solar-to-hydrogen efficiency and current stability with different flow rates. Optical enhancement strategies are shown with rear mirror configuration, RAW long-term stability data. Surface and leaching analyses are provided via XPS and ICP-OES and the custom solar simulator setup is detailed in Figure S15. Literature reports summary on scaled PEC devices (PDF)

Web-Enhanced Feature

The reactor long term operational stability was evaluated under continuous 1 sun illumination at 1.23 V_{RHE} over 120 hours under and constant electrolyte flow (1 mL s⁻¹).

AUTHOR INFORMATION

Corresponding Authors

Ingrid Rodríguez-Gutiérrez — Brazilian Nanotechnology National Laboratory (LNNANO), Brazilian Center for Research in Energy and Materials (CNPEM), Campinas, São Paulo 13083-970, Brazil; ◎ orcid.org/0000-0001-6345-7321; Email: ingrid.gutierrez@lnnano.cnpem.br

Flavio L. Souza — Brazilian Nanotechnology National Laboratory (LNNANO), Brazilian Center for Research in Energy and Materials (CNPEM), Campinas, São Paulo 13083-970, Brazil; Centro de Ciências Naturais e Humanas (CCNH), Federal University of ABC (UFABC), Santo André, São Paulo 09210580, Brazil; Institute of Chemistry, University of Campinas (UNICAMP), Campinas, São Paulo 13083100, Brazil; orcid.org/0000-0003-2036-9123; Email: flavio.souza@lnnano.cnpem.br

Authors

- Lizandra R. P. Peregrino Brazilian Nanotechnology National Laboratory (LNNANO), Brazilian Center for Research in Energy and Materials (CNPEM), Campinas, São Paulo 13083-970, Brazil; orcid.org/0000-0003-3892-9854
- Gabriel H. Morais Brazilian Nanotechnology National Laboratory (LNNANO), Brazilian Center for Research in Energy and Materials (CNPEM), Campinas, São Paulo 13083-970, Brazil; Oorcid.org/0009-0002-3962-469X
- Francine Coa Brazilian Nanotechnology National Laboratory (LNNANO), Brazilian Center for Research in Energy and Materials (CNPEM), Campinas, São Paulo 13083-970, Brazil
- Diego Stéfani Teodoro Martinez Brazilian Nanotechnology National Laboratory (LNNANO), Brazilian Center for Research in Energy and Materials (CNPEM), Campinas, São Paulo 13083-970, Brazil; orcid.org/0000-0002-0086-3055
- Renato V. Gonçalves Instituto de Física de Saão Carlos, Universidade de São Paulo, São Carlos, São Paulo 13566-590, Brazil; orcid.org/0000-0002-3372-6647

Complete contact information is available at: https://pubs.acs.org/10.1021/acsenergylett.5c02340

Author Contributions

The manuscript was written through contributions of all authors. All authors have given approval to the final version of the manuscript.

Funding

The Article Processing Charge for the publication of this research was funded by the Coordenacao de Aperfeicoamento de Pessoal de Nivel Superior (CAPES), Brazil (ROR identifier: 00x0ma614).

Notes

The authors declare no competing financial interest.

ACKNOWLEDGMENTS

The authors acknowledge CNPq (Grant 405727/2022-4), CAPES and FAPESP (Grant 2024/00989-7 and 2017/11986-5), Shell and the strategic importance of the support given by ANP (Brazil's National Oil, Natural Gas and Biofuels Agency) through the R&D levy regulation. The authors are thankful for LNNano facilities.

ABBREVIATIONS

PEC, Photoelectrochemical; Al/Zr, Aluminum/Zirconium; RHE, Reversible Hydrogen Electrode; mA, Milliampere; cm², Square Centimeter; AM, Air Mass; G, Global (solar irradiation); TRL, Technology Readiness Level; ISTC, Intrinsic Solar-to-Chemical Conversion; mW, Milliwatt; 3D, Three-Dimensional; P, Power; $J_{\rm photo}$, Photocurrent Density; $U_{\rm light}$, Light Voltage; $V_{\rm photo}$, Photovoltage

REFERENCES

(1) An, Y.; Lin, C.; Dong, C.; Wang, R.; Hao, J.; Miao, J.; Fan, X.; Min, Y.; Zhang, K. Scalable Photoelectrochemical Cell for Overall Solar Water Splitting into H_2 and H_2O_2 . ACS Energy Lett. **2024**, 9 (4), 1415–1422.

- (2) Mendrela, P.; Stanek, W.; Simla, T. Thermo-Ecological Cost System Evaluation of Energy-Ecological Efficiency of Hydrogen Production from Renewable and Non-Renewable Energy Resources. *Int. J. Hydrogen Energy* **2024**, *50*, 1–14.
- (3) Benavides, K.; Gurgel, A.; Morris, J.; Mignone, B.; Chapman, B.; Kheshgi, H.; Herzog, H.; Paltsev, S. Mitigating Emissions in the Global Steel Industry: Representing CCS and Hydrogen Technologies in Integrated Assessment Modeling. *Int. J. Greenh. Gas Control* **2024**, *131* (March), 103963.
- (4) Von Zuben, T.; Moreira, D.; Germscheidt, R.; Yoshimura, R.; Dorretto, D.; de Araujo, A.; Salles, A., Jr.; Bonacin, J. Is Hydrogen Indispensable for a Sustainable World? A Review of H₂ Applications and Perspectives for the Next Years. J. Braz. Chem. Soc. 2022, 0 (0), 1–20
- (5) Jiang, C.; Moniz, S. J. A.; Wang, A.; Zhang, T.; Tang, J. Photoelectrochemical Devices for Solar Water Splitting Materials and Challenges. *Chem. Soc. Rev.* **2017**, 46 (15), 4645–4660.
- (6) Zghaibeh, M.; Ben Belgacem, I.; Barhoumi, E. M.; Baloch, M. H.; Chauhdary, S. T.; Kumar, L.; Arıcı, M. Optimization of Green Hydrogen Production in Hydroelectric-Photovoltaic Grid Connected Power Station. *Int. J. Hydrogen Energy* **2024**, *52*, 440–453.
- (7) Harris-Lee, T. R.; Marken, F.; Bentley, C. L.; Zhang, J.; Johnson, A. L. A Chemist's Guide to Photoelectrode Development for Water Splitting the Importance of Molecular Precursor Design. *EES Catal.* **2023**, *1* (6), 832–873.
- (8) Vilanova, A.; Dias, P.; Lopes, T.; Mendes, A. The Route for Commercial Photoelectrochemical Water Splitting: A Review of Large-Area Devices and Key Upscaling Challenges. *Chem. Soc. Rev.* **2024**, 53 (5), 2388–2434.
- (9) Tian, K.; Xu, Z.; Yang, H.; Chen, G.; An, P.; Zhang, J.; Liu, S.; Yan, J. Interfacial Engineering-Assisted Energy Level Modulation Enhances the Photoelectrochemical Water Oxidation Performance of Bismuth Vanadate Photoanodes. *Adv. Energy Mater.* **2025**, *15* (12), 1–14.
- (10) Hu, Y.; Shi, Z.; Ren, X.; Cao, Y.; Xiao, G.; Huang, D.; Jiang, F. Boosting Solar Water Splitting Performance of Cu₃BiS₃-Based Photocathode via Ag Doping Strategy. *Adv. Energy Mater.* **2024**, 2402031, 1–9.
- (11) Tian, F.-X.; Sun, S.; Wang, J.-J. Overcoming Acidic Challenges in Hematite Photoanodes: Charge Transport Engineering and Catalytic Interface Optimization. *Small* **2025**, No. e06878.
- (12) Liang, K.; Yang, J.; Ye, M.; Zhang, Y.; Jang, Y. J.; Zhang, H. Hematite Photoanode for Efficient Photoelectrochemical Water Splitting: Recent Advances and Outlook. *Chem. Commun.* **2025**, *61* (43), 7724–7736.
- (13) Li, J.; Chen, H.; Triana, C. A.; Patzke, G. R. Hematite Photoanodes for Water Oxidation: Electronic Transitions, Carrier Dynamics, and Surface Energetics. *Angew. Chemie Int. Ed.* **2021**, *60* (34), 18380–18396.
- (14) Shinagawa, T.; Ng, M. T.; Takanabe, K. Electrolyte Engineering towards Efficient Water Splitting at Mild pH. *ChemSusChem* **2017**, *10* (21), 4122–4122.
- (15) Hankin, A.; Bedoya-Lora, F. E.; Ong, C. K.; Alexander, J. C.; Petter, F.; Kelsall, G. H. From Millimetres to Metres: The Critical Role of Current Density Distributions in Photo-Electrochemical Reactor Design. *Energy Environ. Sci.* **2017**, *10* (1), 346–360.
- (16) Barbera, O.; Lo Vecchio, C.; Trocino, S.; Carbone, A.; Aricò, A. S.; Baglio, V.; Giacoppo, G. Solar to Hydrogen Conversion by a 25 cm²-Photoelectrochemical Cell with Upscaled Components. *Renew. Energy* **2024**, 224, 120154.
- (17) Rodríguez-Gutiérrez, I.; Peregrino, L. R. P.; Bedin, K. C.; Morishita, G. M.; Morais, G. H.; Castro, R. H. R.; Leite, E. R.; Souza, F. L. Overcoming Scale-up Challenges for Nanostructured Photoelectrodes via One-Step Interface Engineering. *Int. J. Hydrogen Energy* **2024**, 58 (Jan), 1138–1148.
- (18) Vilanova, A.; Dias, P.; Azevedo, J.; Wullenkord, M.; Spenke, C.; Lopes, T.; Mendes, A. Solar Water Splitting under Natural Concentrated Sunlight Using a 200 cm² Photoelectrochemical-Photovoltaic Device. *J. Power Sources* **2020**, 454 (Jan), 227890.

- (19) Lee, W. J.; Shinde, P. S.; Go, G. H.; Ramasamy, E. Ag Grid Induced Photocurrent Enhancement in WO₃ Photoanodes and Their Scale-up Performance toward Photoelectrochemical H₂ Generation. *Int. J. Hydrogen Energy* **2011**, *36* (9), 5262–5270.
- (20) Yao, X.; Wang, D.; Zhao, X.; Ma, S.; Bassi, P. S.; Yang, G.; Chen, W.; Chen, Z.; Sritharan, T. Scale-Up of BiVO₄ Photoanode for Water Splitting in a Photoelectrochemical Cell: Issues and Challenges. *Energy Technol.* **2018**, *6* (1), 100–109.
- (21) Lopes, T.; Dias, P.; Andrade, L.; Mendes, A. An Innovative Photoelectrochemical Lab Device for Solar Water Splitting. *Sol. Energy Mater. Sol. Cells* **2014**, *128*, 399–410.
- (22) Vilanova, A.; Lopes, T.; Mendes, A. Large-Area Photoelectrochemical Water Splitting Using a Multi-Photoelectrode Approach. *J. Power Sources* **2018**, 398 (May), 224–232.
- (23) Patil Kunturu, P.; Lavorenti, M.; Bera, S.; Johnson, H.; Kinge, S.; van de Sanden, M. C. M.; Tsampas, M. N. Scaling up BiVO₄ Photoanodes on Porous Ti Transport Layers for Solar Hydrogen Production. *ChemSusChem* **2024**, *17* (2), 1–8.
- (24) Kunturu, P. P.; Bera, S.; Johnson, H.; Tsampas, M. N. Scaled-Up Zero-Gap Photoelectrochemical Device Based on Abundant Materials for Bias-Free Solar Hydrogen Production. *Artif. Photosynth.* **2025**, *1* (2), 106–116.
- (25) Tolod, K.; Hernández, S.; Russo, N. Recent Advances in the BiVO₄ Photocatalyst for Sun-Driven Water Oxidation: Top-Performing Photoanodes and Scale-Up Challenges. *Catalysts* **2017**, *7* (1), 13.
- (26) Qayum, A.; Guo, M.; Wei, J.; Dong, S.; Jiao, X.; Chen, D.; Wang, T. An in Situ Combustion Method for Scale-up Fabrication of BiVO₄ Photoanodes with Enhanced Long-Term Photostability for Unassisted Solar Water Splitting. *J. Mater. Chem. A* **2020**, 8 (21), 10989–10997.
- (27) Ahmet, I. Y.; Ma, Y.; Jang, J. W.; Henschel, T.; Stannowski, B.; Lopes, T.; Vilanova, A.; Mendes, A.; Abdi, F. F.; Van De Krol, R. Demonstration of a 50 cm² BiVO₄ Tandem Photoelectrochemical-Photovoltaic Water Splitting Device. *Sustain. Energy Fuels* **2019**, 3 (9), 2366–2379.
- (28) da Silva Lopes, T.; Dias, P.; Monteiro, R.; Vilanova, A.; Ivanou, D.; Mendes, A. A 25 cm² Solar Redox Flow Cell: Facing the Engineering Challenges of Upscaling. *Adv. Energy Mater.* **2022**, *12* (5), 1–17.
- (29) Miranda, S.; Vilanova, A.; Lopes, T.; Mendes, A. TiO₂-Coated Window for Facilitated Gas Evolution in PEC Solar Water Splitting. *RSC Adv.* **2017**, *7* (47), 29665–29671.
- (30) Thomaz, K. T. C.; Bedin, K. C.; Rodríguez-Gutiérrez, I.; Verissimo, N. C.; Bettini, J.; Souza, F. L. Interfacial Engineering of Hematite Photoanodes toward High Water Splitting Performance. *Mater. Today Energy* **2023**, *37*, 101399.
- (31) Rodríguez-Gutiérrez, I.; Bedin, K. C.; Mouriño, B.; Souza Junior, J. B.; Souza, F. L. Advances in Engineered Metal Oxide Thin Films by Low-Cost, Solution-Based Techniques for Green Hydrogen Production. *Nanomaterials* **2022**, *12* (12), 1957.
- (32) Bedin, K. C.; Mouriño, B.; Rodríguez-Gutiérrez, I.; Junior, J. B. S.; Santos, G. T. d; Bettini, J.; Costa, C. A. R.; Vayssieres, L.; Souza, F. L. Solution Chemistry Back-Contact FTO/hematite Interface Engineering for Efficient Photocatalytic Water Oxidation. *Chin. J. Catal.* 2022, 43 (5), 1247–1257.
- (33) Pires, F. A.; dos Santos, G. T.; Bettini, J.; Costa, C. A. R.; Gonçalves, R. V.; Castro, R. H. R.; Souza, F. L. Selective Placement of Modifiers on Hematite Thin Films for Solar Water Splitting. *Sustain. Energy Fuels* **2023**, *7* (20), 5005–5017.
- (34) Verissimo, N. C.; Pires, F. A.; Rodríguez-Gutiérrez, I.; Bettini, J.; Fiuza, T. E. R.; Biffe, C. A.; Montoro, F. E.; Schleder, G. R.; Castro, R. H. R.; Leite, E. R.; Souza, F. L. Dual Modification on Hematite to Minimize Small Polaron Effects and Charge Recombination for Sustainable Solar Water Splitting. *J. Mater. Chem. A* **2024**, *12* (11), 6280–6293.
- (35) Dias, P.; Vilanova, A.; Lopes, T.; Andrade, L.; Mendes, A. Extremely Stable Bare Hematite Photoanode for Solar Water Splitting. *Nano Energy* **2016**, 23, 70–79.

- (36) Dotan, H.; Mathews, N.; Hisatomi, T.; Grätzel, M.; Rothschild, A. On the Solar to Hydrogen Conversion Efficiency of Photoelectrodes for Water Splitting. *J. Phys. Chem. Lett.* **2014**, *5* (19), 3330–3334.
- (37) Holmes-Gentle, I.; Agarwal, H.; Alhersh, F.; Hellgardt, K. Assessing the Scalability of Low Conductivity Substrates for Photo-Electrodes: Via Modelling of Resistive Losses. *Phys. Chem. Chem. Phys.* **2018**, 20 (18), 12422–12429.
- (38) Vilanova, A.; Lopes, T.; Spenke, C.; Wullenkord, M.; Mendes, A. Optimized Photoelectrochemical Tandem Cell for Solar Water Splitting. *Energy Storage Mater.* **2018**, *13* (Aug), 175–188.
- (39) Holmes-Gentle, I.; Bedoya-Lora, F. E.; Aimone, L.; Haussener, S. Photoelectrochemical Behaviour of Photoanodes under High Photon Fluxes. *J. Mater. Chem. A* **2023**, *11* (44), 23895–23908.
- (40) Li, P.; Kowalczyk, D.; Liessem, J.; Elnagar, M. M.; Mitoraj, D.; Beranek, R.; Ziegenbalg, D. Optimizing Reaction Conditions for the Light-Driven Hydrogen Evolution in a Loop Photoreactor. *Beilstein J. Org. Chem.* **2024**, *20*, 74–91.
- (41) Pereira, E.; Martins, F.; Gonçalves, A.; Costa, R.; Lima, F.; Rüther, R.; Abreu, S.; Tiepolo, G.; Pereira, S.; Souza, J. *Atlas Brasileiro de Energia Solar*; Universidade Federal de São Paulo, 2017; Vol. 2. DOI: 10.34024/978851700089.